Indian Journal of Pure & Applied Physics
Vol. 63, January 2025, pp. 62-69
DOI: 10.56042/ijpap.v63i1.13251

Numerical Simulation of Blood Flow of Casson Fluid with Brownian Motion and Thermophoresis Effect

Laltesh Kumar[a], Atar Singh[a], Vimal K Joshi[b], Dinesh Bhardwaj[c*] & Kushal Sharma[d]

[a]Department of Mathematics, Agra College, Agra 282 004, India

[b]Manipal University Jaipur, Jaipur 303 007, India

[c]Department of Electronics and Communication Engineering, TIET Patiala 147 004, India

[d]Department of Mathematics, MNIT Jaipur, Rajasthan 302 017, India

Received 20 August 2024; accepted 17 December 2024

This research presents a comprehensive numerical investigation into two-dimensional, unsteady blood flow, incorporating the combined effects of thermophoresis and Brownian motion. The study aims to explore how these phenomena influence the dynamics of blood flow under various conditions. To facilitate the analysis, a similarity transformation approach is employed to reduce the complex system of partial differential equations governing the flow into a system of ordinary differential equations. These simplified equations are then solved numerically using a finite difference scheme, with the bvp4c solver in MATLAB and shooting techniques, to obtain both graphical and numerical results. The study specifically examines the effects of several key physical factors on the primary variables of interest in blood flow, including velocity, temperature, and concentration. Through detailed analysis, the research highlights how changes in parameters such as thermophoretic force, Brownian motion, and other relevant factors influence the flow characteristics and behaviour of blood under unsteady conditions. The findings from this investigation have significant practical implications in biomedical applications, including enhancing the understanding of blood flow for blood cancer treatments and improving the effectiveness of magnetic therapies.

Keywords: Casson Fluid; Brownian motion; Thermophoresis; Magnetic field

1 Introduction

Blood flow in the human body is a dynamic process in which heat and mass exchange. The unstable feature refers to fluctuations throughout time, such as pulsatile flow in arteries caused by heartbeat. Understanding how heat and mass transfer occur within blood veins is critical for investigating processes such as drug administration, the transport of oxygen and nutrients, and the removal of metabolic waste products. Heat transmission in MHD Casson fluid[1] flow of blood is affected by blood viscosity, thermal conductivity, and the presence of the magnetic field. The Casson fluid model is often considered to exhibit blood's non-Newtonian behaviour. The Casson fluid model is often considered to exhibit blood's non-Newtonian behaviour. The non-Newtonian fluid flow occurs in many sectors of research, engineering, and food preparation. With this model, Malik *et al.*[2] investigated the MHD flow with varying viscosity over a stretching sheet using a Cattaneo-Christov heat flux model. Sharma and Gaur[3] studied the heat-mass transfer phenomena on pulsatile bio-magnetic MHD flow of blood, assuming variable viscosity and chemical reaction. The effect of numerous constraints like Reynolds number, hydromagnetic parameter, variable viscosity, and Prandtl number on flow behaviour can be visualized using some computational models and numerical simulations[4-11] to investigate non-Newtonian fluid flows such as blood. Sarma & Paul[12] investigated the flow of engine oil blended Casson hybrid nanofluid over a uniformly heated curved surface, incorporating the effects of magnetic field alignment, activation energy, and suction.

Solutes (such as oxygen, carbon dioxide, and nutrients) may be transported through the bloodstream as part of mass transfer in blood flow. The magnetic field can impact the diffusion and convection of solutes in blood in an MHD environment. To comprehend temperature distribution in biological systems and medical applications, heat transfer analysis in blood flow is crucial. Nazar *et al.*[13] discussed the heat transfer effect on mixed steady flow in a porous medium over an

*Corresponding author: (E-mail: dinesh.bhardwaj@thapar.edu)

isothermal horizontal circular cylinder. Zhao *et al.*[14] investigated the MHD stagnation point flow of nanofluid across a stretchable surface under impacts of chemical reaction and thermal radiation. The examination of ferrohydrodynamic fluid flow across a rotating disc with temperature-dependent thermal conductivity and geothermal viscosity that is directly proportional to the linear relationship of depth and inversely proportional to temperature is studied by Sharma *et al.*[15]. With this geometry, Sharma *et al.*[16] recently studied the influence of porosity with forced convective heat transfer on steady ferrohydrodynamic flow for a water-based magnetic nanofluid across a rotating disc. Paul *et al.*[17] numerically discussed the thermal and mass transfer characteristics of Casson-Maxwell hybrid nanofluids flowing through an unsteady horizontal cylinder, incorporating variable thermal conductivity and Arrhenius activation energy. Furthermore, Paul *et al.*[18] investigated the 3D MHD flow of Casson $Cu-TiO_2-SiO_2$/transformer oil ternary hybrid nanofluid incorporating effects such as Hall current, thermophoresis, and thermal radiation. Their study reveals significant enhancements in heat and mass transfer rates, with practical implications for rotating machinery, medical devices, and gas turbines. Many researchers[19-24] examined the consequences of radiation, thermal diffusion, and diffusion-thermo on the flow of a nanofluid over a stretching sheet. The investigation of heat and mass transfer of MHD Casson fluid flow of blood past a porous stretching/shrinking sheet is shown in the present work under the influence of Brownian motion and thermophoresis effects. Using similarity variables, the governing equation system is converted to an ODE. The findings are presented via graphs and tables. The present study's key goals are as follows:

a) What are the physical implications of 2-dimensional unstable blood flow?

b) How does the porous lumen lining the walls of the blood affect liquid velocity?

c) What are the consequences of the modelled physical factors on flow variables in the problem?

d) How do the Brownian motion and thermophoresis affect the transport phenomena?

2 Mathematical Formulation

2.1 Casson's Fluid Rheology

The Casson fluid model describes the relationship between the stress and strain rate tensor under different stress conditions. Important factors like μ_B (plastic dynamic viscosity of fluid), p_y (permits fluid stress), and π_c (critical value based on the Casson fluid model) are employed in Casson fluid flow using the Rheological equation.

$$\tau_{ij} = \begin{cases} 2\left(\mu_B + \frac{p_y}{\sqrt{2\pi}}\right) e_{ij}\,, & \pi > \pi_c \\ 2\left(\mu_B + \frac{p_y}{\sqrt{2\pi_c}}\right) e_{ij}\,, & \pi < \pi_c \end{cases} \quad \ldots (1)$$

When the applied stress exceeds the critical value ($\pi > \pi_c$), the fluid flows and shows a characteristic shear-thinning behaviour. When applied stress is less than the critical value ($\pi < \pi_c$), the fluid does not flow and acts more like a solid.

2.2 Flow Description

An unstable two-dimensional MHD Casson fluid (blood) flow of an incompressible viscous thermal radiant is studied across a shrinking/stretching sheet Fig. 1. The chemical reaction, along with Brownian motion and thermophoresis, are also taken into consideration. The rheological equation of state for an isotropic and incompressible Casson fluid flow is typically stated[25].

The governing system of equations is as follows:

$$\frac{\partial u}{\partial x} + \frac{\partial v}{\partial y} = 0. \quad \ldots (2)$$

$$\frac{\partial u}{\partial t} + u\frac{\partial u}{\partial x} + v\frac{\partial u}{\partial y} = \frac{1}{\rho}\frac{\partial p}{\partial x} + \upsilon\left(1 + \frac{1}{\beta}\right)\frac{\partial^2 u}{\partial y^2} - \left(\frac{\sigma {B_0}^2}{\rho}u - \frac{\nu}{K_1(t)}u\right) + g\beta_T(T - T_\infty) + g\beta_C(C - C_\infty). \quad \ldots (3)$$

$$\frac{\partial T}{\partial t} + u\frac{\partial T}{\partial x} + v\frac{\partial T}{\partial y} = \alpha\frac{\partial^2 T}{\partial y^2} - \frac{1}{\rho C_p}\frac{\partial q_r}{\partial y} + \tau\left\{D_B\frac{\partial C}{\partial y}\frac{\partial T}{\partial y} + \frac{D_T}{T_\infty}\left(\frac{\partial^2 T}{\partial y^2}\right)\right\}. \quad \ldots (4)$$

$$\frac{\partial C}{\partial t} + u\frac{\partial C}{\partial x} + v\frac{\partial C}{\partial y} = D_B\frac{\partial^2 C}{\partial y^2} - K_r{}^*(C - C_\infty) + \frac{D_T}{T_\infty}\left(\frac{\partial^2 T}{\partial y^2}\right). \quad \ldots (5)$$

From the above equations, $\alpha = \frac{k}{\rho C_p}$, where α is thermal diffusivity, k represents thermal conductivity, ρ represents density, (C_p) represents specific heat at constant pressure (p) and kr^* denotes chemical reaction. Here, molecular diffusivity (D_B) represents the rate at which species and particles diffuse through the fluid due to concentration gradients.

Important boundary circumstances of the model (Sitamahalakshmi *et. al*[26]) can be written as,

$$\left.\begin{array}{l} u = U_w, v = f_w, T = T_w, C = C_w \text{at } y = 0, \\ u = 0,\ T \to T_\infty,\ C \to C_\infty \quad \text{as } y \to \infty. \end{array}\right\} \quad \ldots (6)$$

In Eq. (6), blood velocity at the wall is f_w (for suction:$f_w < 0$, and for injection:$f_w > 0$) and is given as,

$$f_w = -\sqrt{\left(\frac{vV_w}{x}\right)S}. \quad \ldots (7)$$

In Eq. (3), the time-dependent permeable parameter $K_1(t) = K_2(t)\,(1 - ct)$ defines the porosity behaviour over time. The stretching velocity of the blood vessel, surface temperature, blood concentration, and the time-dependent chemical reaction parameter $K_r(t)$ are defined as follows:

$$U_w(x,t) = \frac{ax}{1-ct}, \qquad T_w(x,t) = T_\infty + \frac{bx}{1-ct},$$
$$C_w(x,t) = C_\infty + \frac{bx}{1-ct},\ K_r(t) = \frac{K_r^*}{1-ct}. \quad \ldots (8)$$

Here a, b, c and K_r^* are constants with $a > 0,\ b \geq 0,\ c \geq 0$, and $ct < 1$ to ensure stability over time. Also, $B(t) = \sqrt{(B_0 / (1 - \mathrm{ct}))}$, where B_0 is the magnetic field strength at $t = 0$.

The Rosseland approximation[27] provides heat radiation(q_r), and is given by

$$q_r = -\frac{4\sigma^*}{3K^m}\frac{\partial T^4}{\partial y}, \quad \ldots (9)$$

where, $\sigma^*$is the Stefan-Boltzmann constant, which is equal to $5.67 \times 10^{-8}\, W/m^2K^4$ and K^m is the Roseland mean absorption coefficient. If the temperature difference around the blood flow is sufficiently small, T^4 in Eq. (9) can be approximated by expanding T^4 in a Taylor series about T_∞ and neglecting higher-order terms, yielding:

$$T^4 \cong 4T_\infty^3 T - 3T_\infty^4. \quad \ldots (10)$$

The stream function Ψ is used for the velocity components such as $u = \frac{\partial \Psi}{\partial y}$, $v = -\frac{\partial \Psi}{\partial x}$to simplify the continuity equation. Furthermore, to simplify the governing equations, the dimensionless similarity variable (η) and dimensionless functions $f(\eta),\ \theta(\eta)$ and $\phi(\eta)$ are taken as follows:

$$\eta = \left(\frac{U_w}{\nu x}\right)^{\frac{1}{2}} y, \quad \Psi = f(\eta)\sqrt{\nu x U_w}\ ,$$
$$\theta(\eta) = \frac{T-T_\infty}{T_w-T_\infty}, \quad \phi(\eta) = \frac{C-C_\infty}{C_w-C_\infty}. \quad \ldots (11)$$

By using Eq. (11), the system of Eqs. (3-5) is reduced into nonlinear coupled ODEs such as:

$$\left(1+\frac{1}{\beta}\right)f''' + ff'' - f'^2 - \left(M + \frac{1}{K}\right)f' -$$
$$A(f' + 0.5\eta f'') + \lambda_T\theta + \lambda_m\phi = 0 \quad \ldots (12)$$

$$(1+R)\theta'' + Pr\left(f\theta' - f'\theta - Scf\phi' - Scf'\phi -\right.$$
$$\left. ScA(\phi + 0.5\eta\theta') + Nb\theta'\phi' + Nt\theta'^2\right) = 0 \quad \ldots (13)$$

$$\phi'' + Scf\phi' - Scf'\phi - ScA(\phi + 0.5\eta\phi') - K_r\phi +$$
$$\left(\frac{Nt}{Nb}\right)\theta'' = 0. \quad \ldots (14)$$

Subject to

$$\left.\begin{array}{l} f = S,\ f' = 1,\ \theta = 1,\ \phi = 1 \quad at \quad \eta = 0 \\ f' \to 0,\ \theta \to 0,\ \phi \to 0 \qquad as \quad \eta \to \infty \end{array}\right\}, \quad \ldots (15)$$

where, $A = \frac{c}{a}, a = \nu(1 - ct),\ M = \frac{xB_0^2\sigma}{\rho U_w}$,

$$R = \frac{16\sigma^* T_\infty^3}{3K^m}, \quad K = \frac{aK_1}{\nu}, \quad Sc = \frac{\upsilon}{D_B}, \quad Pr = \frac{\upsilon}{\alpha},$$

$$\lambda_T = \frac{Gr}{Re_x^2} = \frac{g\beta_T(T_w - T_\infty)}{x\,\nu^2(1 - ct)}, \quad \lambda_m = \frac{Gc}{Re_x^2} = \frac{g\beta_c(C_w - C_\infty)}{(1 - ct)x\,\nu^2},$$

$$Nt = \frac{(T_w - T_\infty)\tau D_T}{\nu T_\infty}, \quad Nb = \frac{(C_w - C_\infty)\tau D_B}{\nu},$$

$$Re_x = \frac{U_w x}{\nu}, \quad K_r = \frac{xK_r^*}{U_w}.$$

2.3 Physical Parameters of Engineering Interest

The skin-friction coefficient, Nusselt, and Sherwood numbers (Table 1) are used to characterize fluid flow friction on boundary layer, heat, and mass transmission. These non-dimensional parameters are important in fluid dynamics and heat/mass transfer analyses because they allow engineers and researchers to compare and predict the behaviour of fluids and heat/mass transfer across different geometries and conditions without having to consider the fluid's specific properties or system size. These dimensionless parameters are given by,

Coefficient of skin friction, $C_f = -\left(1 + \frac{1}{\beta}\right)f''(0).$

Nusselt Number, $N_u = -(1+R)\theta'(0).$

Sherwood Number, $S_h = -\phi'(0).$

3 Methodology

The basic equations in our model were turned into ODEs using the mandatory similarity variables, and they were then numerically solved in "MATLAB" software. A comparison table (Table 2) is also given for the code validation of the method used. Following is a description of the problem with conditions:

Table 1 — Local Skin-Friction Coefficient, Nusselt Number & Sherwood Number.

$\boldsymbol{M}$	K	β	Pr	Sc	Kr	Nt	Nb	C_f	N_u	S_h
0.2	0.5	0.5	0.71	0.6	0.2	0.2	0.1	0.8826	0.9742	0.04888
0.5								0.9008	0.9701	0.04836
1								0.9303	0.9634	0.04748
0.2	0.2	0.5	0.71	0.6	0.2	0.2	0.1	1.0500	0.9370	0.04345
	0.5							0.8826	0.9742	0.04888
	1							0.8188	0.9888	0.05054
0.2	0.5	0.2	0.71	0.6	0.2	0.2	0.1	0.6105	1.0380	0.05391
		0.5						0.8826	0.9742	0.04888
		1						1.1020	0.9259	0.04149
0.2	0.5	0.5	0.71	0.6	0.2	0.2	0.1	0.9956	0.9399	0.8513
			1					0.9956	1.2200	0.1635
			7					0.9956	6.386	5.9970
0.2	0.5	0.5	0.71	0.22	0.2	0.2	0.1	0.8826	0.8264	0.1788
				0.3				0.8826	0.8264	0.1849
				0.78				0.8826	0.8264	0.2116
0.2	0.5	0.5	0.71	0.22	0.5	0.2	0.1	0.8826	0.8270	0.2187
					1			0.8826	0.8279	0.2795
					2			0.8826	0.8295	0.3851
0.2	0.5	0.5	0.71	0.22	0.5	0.1		0.4348	1.900	2.94343
						0.2		0.4242	1.912	2.96791
						0.4		0.4067	1.989	3.00720
0.2	0.5	0.5	0.71	0.22	0.5	0.1	0.3	1.4008	2.122	2.89413
							0.5	0.8882	2.201	2.93068
							1.0	0.4408	2.246	2.92965

Table 2 — Comparison table of the present study when $\boldsymbol{\beta = Sc = Kr = 0}$.

$\boldsymbol{M}$	Pr	Sitamahalakshmi *et al.*[26]	Present study
		$-\theta'(0)$	$-\theta'(0)$
0.5	0.21	0.4659	0.4885
0.5	0.25	0.5335	0.5405
0.5	0.21	0.3294	0.3464
1.0	0.21	0.4242	0.4348
0.5	0.21	0.3904	0.4013

$$f = \widetilde{y_1}, \quad f' = \widetilde{y_2}, \quad f'' = \widetilde{y_3}, \quad \theta = \widetilde{y_4}, \quad \theta' = \widetilde{y_5}, \quad \phi = \widetilde{y_6}, \quad \phi' = \widetilde{y_7},$$

$$\widetilde{y_1}' = \widetilde{y_2}, \widetilde{y_2}' = \widetilde{y_3},$$

$$\widetilde{y_3}' = \left(\frac{\beta}{1+\beta}\right) * (\widetilde{y_2^2} - \widetilde{y_1} * \widetilde{y_3} + (A) * \widetilde{y_2} + 0.5 * n * \widetilde{y_3} - L * \widetilde{y_4} - Z * \widetilde{y_6} + K * \widetilde{y_5} + \frac{M}{1+K} * \widetilde{y_2} - L * \widetilde{y_4} - Z * \widetilde{y_6},$$

$$\widetilde{y_4}' = \widetilde{y_5},$$

$$\widetilde{y_5}' = \left(\frac{1}{1+R}\right) * (-Pr * \widetilde{y_1} * \widetilde{y_5} - \widetilde{y_4} * \widetilde{y_2} - A * (\widetilde{y_4} * 0.5 * n * \widetilde{y_5}) - Nb * \widetilde{y_5} * \widetilde{y_7} - Nt * \widetilde{y_5^2},$$

here, $A = \left(1 + \frac{4}{3} * Rd - Sc * Pr * Du * Sr\right)$;

$$\widetilde{y_6}' = \widetilde{y_7},$$

$$\widetilde{y_7}' = (Sc) * (\widetilde{y_1} * \widetilde{y_7} + \widetilde{y_2} * \widetilde{y_6}) + A * (\widetilde{y_6} + 0.5 * n * \widetilde{y_7} + Kr * \widetilde{y_6} - \left(\frac{Nt}{Nb} * \left(\frac{1}{1+R}\right)\right) * (-Pr * \widetilde{y_1} * \widetilde{y_5} - \widetilde{y_4} * \widetilde{y_2} - A * \widetilde{y_4} * 0.5 * n * \widetilde{y_5} - Nb * \widetilde{y_5} * \widetilde{y_7} - Nt * \widetilde{y_5^2}),$$

$$\widetilde{y_9} = (-Sc) * (\widetilde{y_1} * \widetilde{y_9} + Sc * Kn * \widetilde{y_8}).$$

Subject to the subsequent boundary circumstances

$$\widetilde{y_1} = S, \widetilde{y_2} = \varepsilon, \quad \widetilde{y_4} = 1, \quad \widetilde{y_6} = 1 \ as\ \eta = 0;$$
$$\widetilde{y_2} = 0, \quad \widetilde{y_4} = 0, \quad \widetilde{y_6} = 0 \quad as\ \eta \text{ tends to infinite.}$$

4 Results and Discussion

In this study, a theoretical analysis of Casson fluid flow for blood is performed by considering the heat-mass transport phenomenon. We have imposed the magnetism of uniform strength to the flow direction because the blood as a Casson fluid considered in this study is electrically conducting. Furthermore, velocity, temperature, and concentration distributions were examined, and the effects of various relevant flow parameters were demonstrated.

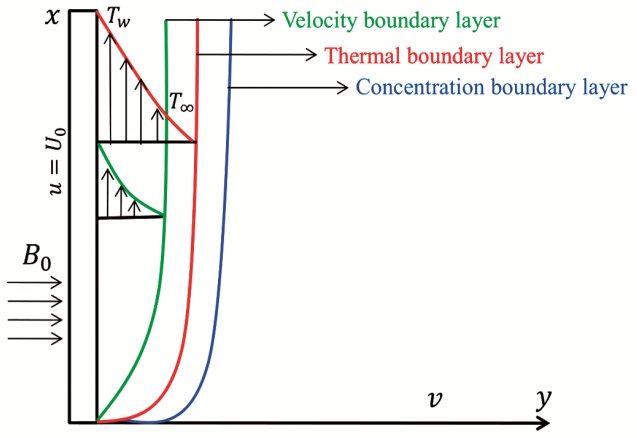

Fig. 1 — Geometry of the physical model

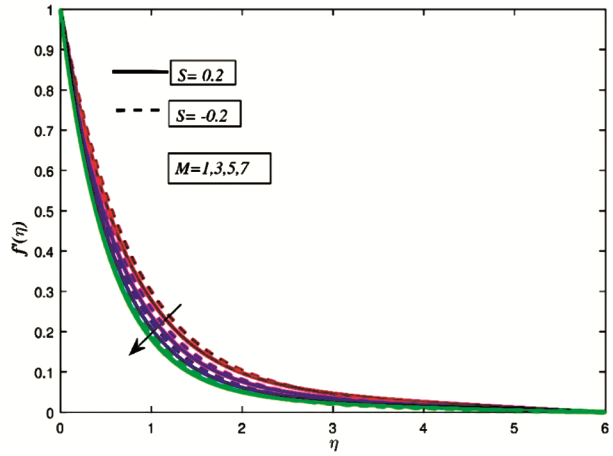

Fig. 2 — Magnetization *vs* Velocity Profile

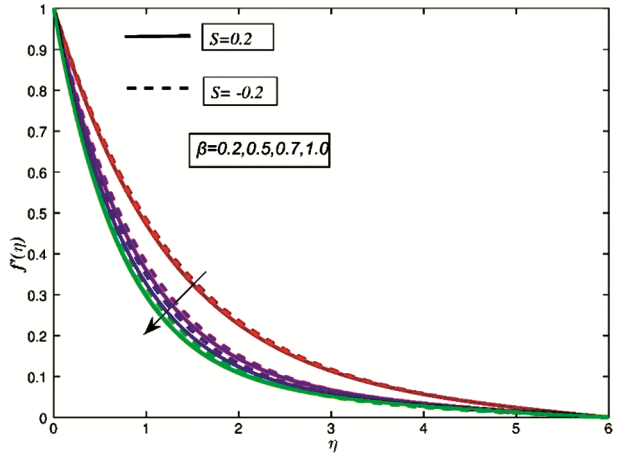

Fig. 3 — Casson Fluid Parameter *vs* Velocity Profile

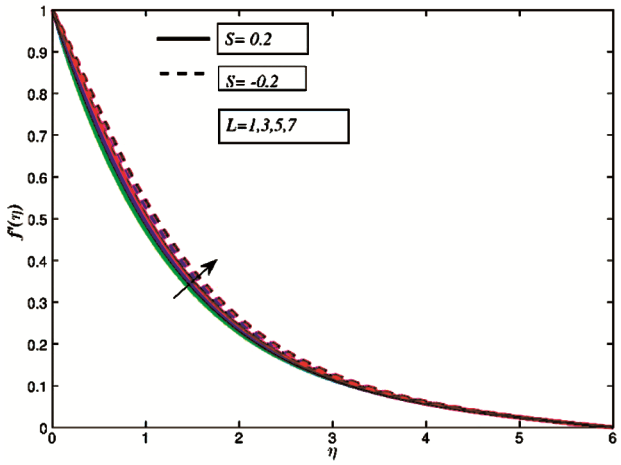

Fig. 4 — Thermal Grashof Number *vs* Velocity Profile

4.1 Variation of Velocity Profile

Figures (2-6) represent the flow behaviour of Casson fluid influenced by the physical parameters, namely magnetic parameter (M), Cassion fluid parameter (β), Grashof number (L), material parameter (K) and buoyancy factor (z), respectively. Figs. (2-3) indicate the slower fluid flow on increasing the value of magnetic as well as the Casson fluid parameter. The intense (higher value) magnetization provides a physical retardation force that is directed in the opposite direction of the flow. Also, the higher Casson fluid parameter is responsible for more viscous force, resulting in more friction and prevention in the flow velocity.

Fig. 4 shows the impact of the thermal Grash of number L for velocity profile. When the Grashof number increases, the buoyancy forces become more significant, promoting the upward motion of the fluid and increasing the velocity. As the material parameter increases (Fig. 5), the viscosity of the fluid decreases, leading to an increase in velocity due to reduced flow resistance. The buoyancy factor (Z) represents the effect of solutal buoyancy on the flow (Fig. 6). When the buoyancy factor increases, the density difference between the fluid and the surrounding environment becomes more pronounced, causing the fluid to rise more easily and thus reduce viscous resistance. This increase in buoyant forces accelerates the flow.

4.2 Variation of Temperature Profile

Temperature profile for distinct Prandtl number, Brownian motion, and thermophoresis for $S = -0.2, 0.2$ are sketched in Figs (7-9). With a high Prandtl number, the thermal diffusivity is lower. As a result (Fig. 7), the thermal boundary layer thickens, which hinders heat transfer and leads to a lower temperature in the fluid. Fig. 8 depicts how Brownian motion influences temperature curves. The more intense Brownian motion causes energy dispersion

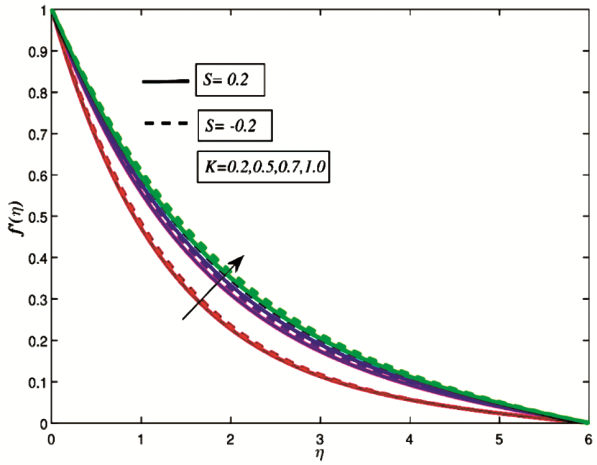

Fig. 5 — Material Factor *vs* Velocity Profile

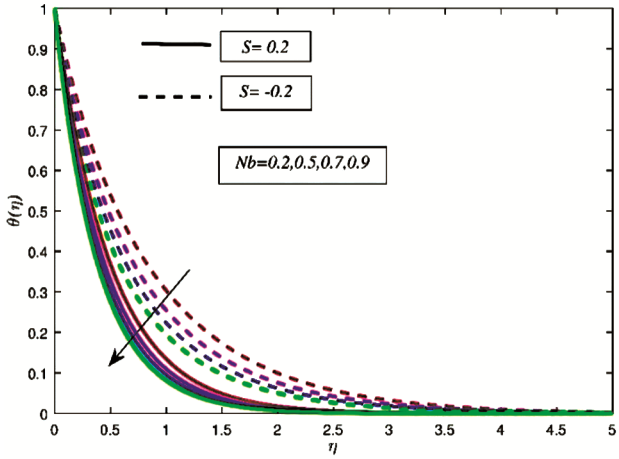

Fig. 8 — Brownian Motion *vs* Temperature Profile

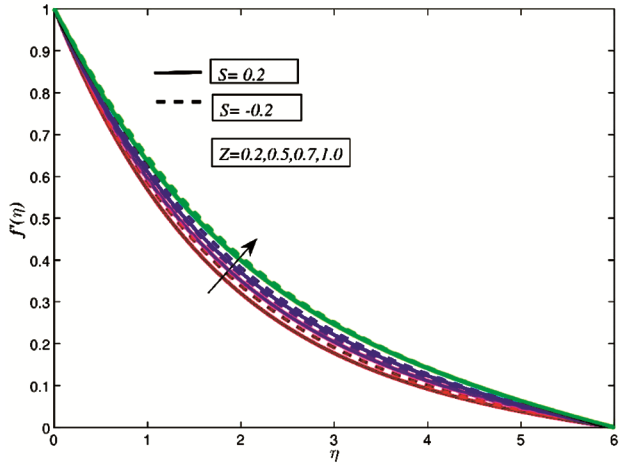

Fig. 6 — Solutal Buoyancy Factor *vs* Velocity Profile

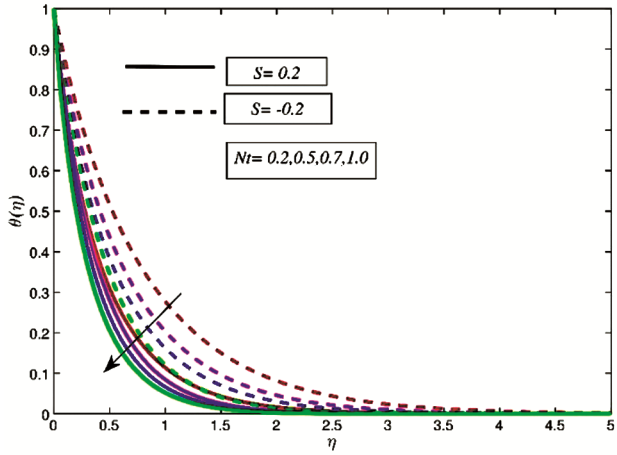

Fig. 9 — Thermophoresis *vs* Temperature Profile

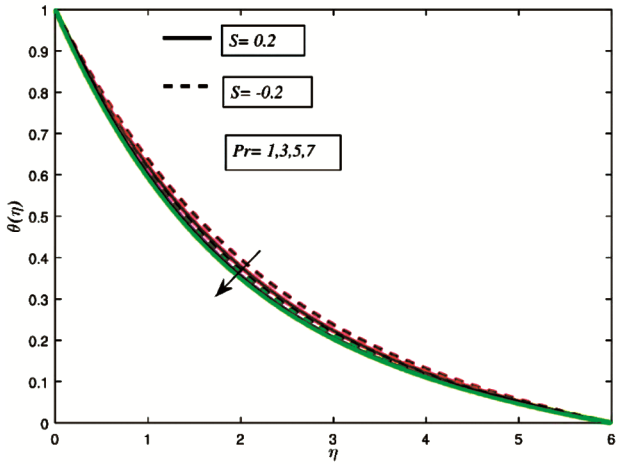

Fig. 7 — Prandtl Number *vs* Temperature Profile

across the fluid, thus lowering the temperature. The thermophoresis parameter (Nt) characterizes the tendency of particles to move from regions of high temperature to low temperature. As Nt increases (Fig. 9), the rate of nanoparticle migration increases, which results in a reduced local temperature of the fluid.

4.3 Variation of Concentration Profile

Figure 10 displays how the unsteadiness parameter affects the Casson fluid's concentration curves. Both cases, the stretching (S = 0.2) and shrinking (S = – 0.2) showed that when the value of *A* increases, the blood particle species concentration field shrinks. As a result, a remarkable loss in the concentration boundary layer thickness is observed. Fig. 11 depicts the chemical reaction impact on the concentration profile of the Casson fluid. As Kr increases, the reaction rate intensifies, causing the chemically reactive species to be consumed more rapidly. This leads to a decrease in concentration near the surface because the reaction effectively removes the particles from the flow. Moreover, the increasing Schmidt

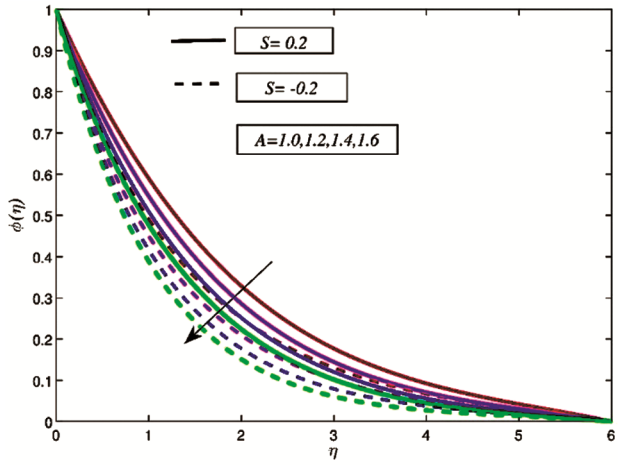

Fig. 10 — Unsteadiness Parameter *vs* Concentration Profile

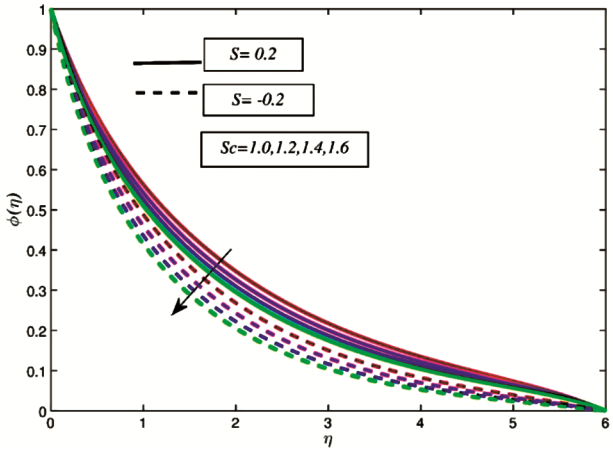

Fig. 12 — Schmidt Number *vs* Concentration Profile

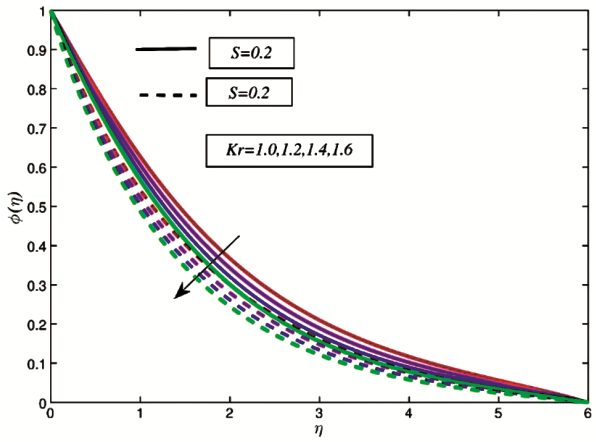

Fig. 11 — Chemical Reaction *vs* Concentration Profile

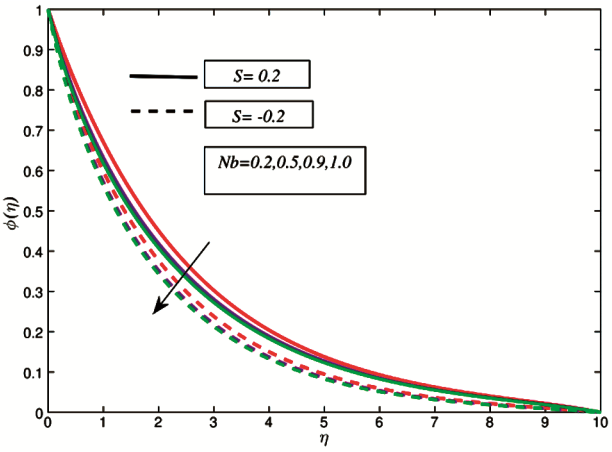

Fig. 13 — Brownian Motion *vs* Concentration Profile

number shows the reverse trend for the fluid flow (Fig. 12). In contrast, a lower Schmidt number indicates more efficient mass transfer, leading to a thinner concentration layer and faster dispersion of the particle species in the fluid. The consequences of the Brownian motion parameter on concentration profiles are seen in Fig. 13. It is noted that as the Brownian motion increases, the random motion of the particles becomes more pronounced, which causes the particles to disperse more effectively. This leads to a reduction in the concentration of the solute in the vicinity of the surface.

The thermophoresis effect refers to the migration of particles from regions of higher temperature to regions of lower temperature due to the temperature gradient. Fig. 14 illustrates the impact of the thermophoresis parameter (Nt) on the concentration profile. As the thermophoresis parameter (Nt) increases, the concentration profile improves, showing an enhancement in the mass transfer process.

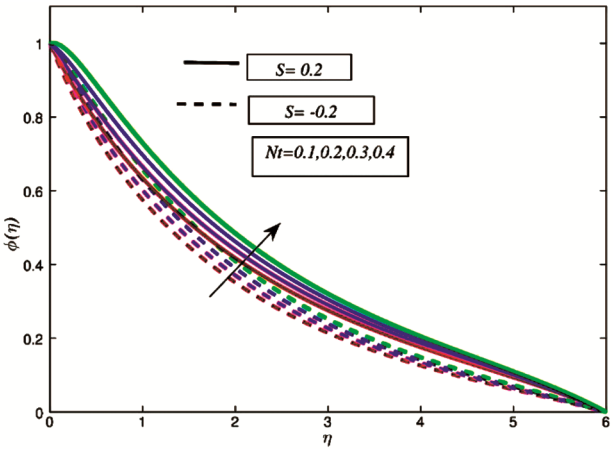

Fig. 14 — Thermophoresis *vs* Concentration Profile

5 Conclusion

The numerical investigation of the two-dimensional unsteady MHD Casson fluid flow of blood across a porous lumen lining wall of the blood is presented in this investigation. The chemical

reaction with Brownian motion and thermophoretic effects are included to describe the Casson fluid behaviour of blood. The governing nonlinear equation of motion, microrotation, temperature and concentration are solved by using the bvp4c method in "MATLAB" software. The findings of the recent investigation are summarized as below:

1 Increasing the magnetic field strength and Casson fluid parameter slows fluid flow by raising viscosity and friction, which hinders velocity.
2 Higher Grashof numbers enhance buoyancy and fluid velocity, while Prandtl number thickens the thermal boundary layer, reducing heat transfer. Additionally, Brownian motion and thermophoresis improve mass and heat transfer by dispersing particles.
3 Chemical reaction parameter reduces surface concentration by accelerating solute consumption, while the Schmidt number and Brownian motion impact the concentration boundary layer and mass transfer efficiency.

These insights can optimize nanofluid-based systems for a wide range of industrial, biomedical, and environmental applications, therapeutic treatments, diagnostic tools, and medical device design, offering more efficient and targeted solutions in cancer treatment, drug delivery, cooling systems, and biomaterial development. The insights gained from this study may lead to more effective medical treatments and advanced diagnostic techniques in these areas.

References

1 Dash R K, Mehta K N & Jayaraman G, *Int J Eng Sci*, 34(1996) 1145.
2 Malik M Y, Khan M, Salahuddin T & Khan I, *Eng Sci Tech Int J*, 19 (2016) 1985.
3 Sharma M & Gaur R K, *Glob J Pure Appl Math*, 13 (2017) 26.
4 Ullah I, Bhattacharyya K, Shafie S & Khan I, *PLOS ONE*, 11 (2016) e0165348.
5 Mabood F & Das K, *Heliyon*, 5 (2019) e01216.
6 Abbas T, Rehman S, Shah R A, Idrees M & Qayyum M, *Phys A Stat Mech Appl*, 551 (2020), 124225.
7 Vinodkumar R M, Lakshminarayana P & Vajravelu K, *Comput Thermal Sci*, 12 (2020) 317.
8 Reddy N N, Srinivasa Rao V & Ravindra R B, *Case Stud Therm Eng*, 25 (2021) 100879.
9 Vinodkumar R M & Lakshminarayana P, *Top Rev Porous Media Int J*, 12 (2021) 33.
10 Vijay N & Sharma K, *Multidiscip Model Mater Struct*, 19 (2023) 253.
11 Saleem M & Hussain M, *Res Eng*, 17 (2023) 100864.
12 Sarma N & Paul A, *Hybrid Adv*, 5 (2024) 100161.
13 Nazar R, Tham L, Pop I & Ingham D B, *Trans Porous Media*, 86 (2011) 517.
14 Zhao T, Khan M, Chu Y, Issakhov I, Ali R & Khan S, *Appl Math Mech Engl Ed*, 42 (2021) 1205.
15 Sharma K, Vijay N, Mabood F & Badruddin I, *Int Commun Heat Mass Transfer*, 133 (2022) 105977.
16 Sharma K, Kumar S, Narwal A, Oudina F M & Animasaun I L, *Int J Appl Comput Math*, 8 (2022) 159.
17 Paul A, Sarma N & Patgiri B, *Numer Heat Transfer, Part A: Appl*, (2023).
18 Paul A, Patgiri B & Sarma N, *ZAMM-Zeitschrift Angewandte Mathematik Mechanik*, 104 (2024) 202300704.
19 Mahanthesh B, Gireesha B J & Gorla R S R, *J Nanofluids*, 5 (2016) 669.
20 Falodun B O, Ayoade A A & Odetunde O, *Australian J Mech Eng*, 21 (2023) 965.
21 Siddique I, Nadeem M, Awrejcewicz J & Pawlowski W, *Sci Rep*, 12 (2022) 11811.
22 Ahmed B, Akbar F, Ghaffari A, Khan S U, Khan M I & Reddy Y D, W*aves Random Complex Media*, (2022). http://dx.doi.org/10.1080/17455030.2022.2085891.
23 Kumar M A, Reddy Y D, Goud B S & Rao V S, *Int J Ambient Energy*, 43 (2022) 7410.
24 Patgiri B, Paul A & Sarma N, *Multidiscip Model Mater Struct*, 20 (2024) 688.
25 Sharma K, Kumar L, Singh A & Joshi V K, *MPLB*, 38 (2024) 2341007.
26 Sitamahalakshmi V, Reddy G V R & Falodun B O, *J Appl Nonlinear Dynamics*, 12 (2023) 87.
27 Sharma K, Vijay N, Ram D & Animasaun I L, *Numer Heat Transf A: Appl*, 84 (2023) 980.